Journal of Catalysis 301 (2013) 198–209

Contents lists available at SciVerse ScienceDirect

Journal of Catalysis

journal homepage: www.elsevier.com/locate/jcat

Structure sensitivity via decoration of low-coordination exposed metal atoms: CO oxidation catalysis on Pt clusters

Mónica García-Diéguez [a], Enrique Iglesia [a,b,*]

[a] Department of Chemical Engineering, University of California at Berkeley, Berkeley, CA 94720, USA
[b] Division of Chemical Sciences, E.O. Lawrence Berkeley National Laboratory, Berkeley, CA 94720, USA

ARTICLE INFO

Article history:
Received 21 November 2012
Revised 31 January 2013
Accepted 13 February 2013
Available online 22 March 2013

Keywords:
Structure sensitivity
CO oxidation
Platinum
Oxygen decoration

ABSTRACT

The effects of CO and O_2 concentrations on turnover rates and $^{18}O_2$–$^{16}O_2$ exchange rates during catalysis are used to assess the relevant elementary steps and the consequences of Pt coordination for CO oxidation catalysis at moderate temperatures (700–800 K) on supported Pt clusters 1.8–25 nm in diameter. Turnover rates, measured under conditions of strict kinetic control, are proportional to O_2 pressure and inhibited by CO; these data are consistent with kinetically-relevant O_2 dissociation steps on cluster surfaces covered partially by chemisorbed CO (CO^*). O_2 dissociation also limits CO oxidation rates at higher temperatures, which lead to bare Pt surfaces, and at lower temperatures, where saturation CO^* coverages require O_2 dissociation to be assisted by CO^* because of a dearth of vacant sites. At the intermediate temperatures used here, kinetic coupling between irreversible O_2 activation and CO^* reactions with O^* causes edge and corner atoms to become decorated by unreactive O^* species; consequently, turnovers occur predominantly on exposed low-index planes, which account for a decreasing fraction of exposed atoms with increasing metal dispersion. These decoration effects confer the appearance of structure sensitivity to the prototypical structure insensitive reaction by rendering only a fraction of exposed metal atoms able to turnover. These active sites, residing at exposed low-index planes, show similar CO^* binding energies on large and small Pt clusters, but their relative abundance decreases as clusters become smaller, leading to a sharp decrease in turnover rates with increasing Pt dispersion. These trends stand in marked contrast with the absence of cluster size effects on CO oxidation rates at low temperatures, where high CO^* coverages dampen the intrinsic site non-uniformity of metal clusters, and at high temperatures, where all Pt atoms remain accessible irrespective of coordination and active for catalytic turnovers.

1. Introduction

The catalytic oxidation of CO has been widely studied at low temperatures (360–473 K) because of its relevance in the removal of CO from H_2-rich streams [1–3] and from automotive exhaust [4,5]. Fewer studies are available at higher temperatures, in spite of its importance in the oxidation of trace CO components in combustion effluent streams [6,7]. Its molecular simplicity and detectable rates over a wide temperature range have made this reaction a ubiquitous choice in probing fundamental concepts in heterogeneous catalysis and specifically the effects of cluster size and surface coordination on catalytic reactivity [1,3].

At low temperatures, CO oxidation occurs on surfaces nearly saturated with chemisorbed CO (CO^*), but CO^* coverages decrease with increasing temperature and unoccupied surface atoms ($*$) ultimately replace CO^* as the most abundant surface intermediates (MASI). On surfaces covered with CO^*, turnover rates depend weakly on Pt cluster size [3,8], because CO^* monolayers appear to dampen the consequences of the intrinsic non-uniformity of small Pt clusters, which would be expected to cause strong size effects [9]. Such non-uniformity is likely to become increasingly influential as surface atoms with varying coordination and binding properties become accessible at lower CO^* coverages.

Kinetic, isotopic, and infrared data and their mechanistic interpretation indicate that CO oxidation at low temperatures (350–450 K) on Pt proceeds via kinetically-relevant O_2 activation steps assisted by CO^* [3], consistent with the effects of CO and O_2 concentrations on turnover rates:

$$r_{CO} = \frac{K_{O_2} k_{O_2^*-CO^*}}{K_{CO}} \frac{[O_2]}{[CO]} = k_{eff} \frac{[O_2]}{[CO]} \quad (1)$$

In this equation, $k_{O_2^*-CO^*}$ is the rate constant for the activation of O_2^* assisted by interactions with vicinal CO^* species and K_{O_2} and K_{CO} are the equilibrium constants for the molecular adsorption of O_2 and CO, respectively. At low O_2/CO ratios, CO^* can instead react with another CO^* to form CO_2 and chemisorbed carbon (C^*) [10]. At these

* Corresponding author at: Department of Chemical Engineering, University of California at Berkeley, Berkeley, CA 94720, USA. Fax: +1 510 642 4778.
E-mail address: iglesia@berkeley.edu (E. Iglesia).

0021-9517/$ - see front matter © 2013 Elsevier Inc. All rights reserved.
http://dx.doi.org/10.1016/j.jcat.2013.02.014

low temperatures, turnover rates and activation energies depend only weakly on Pt cluster size (1.2–20.0 nm) [3,8], in spite of marked differences in the average coordination of exposed Pt atoms in clusters within this size range. It appears that the binding properties of isolated vacancies within dense CO* overlayers depend strongly on intermolecular interactions but much more weakly on the coordination of exposed metal atoms [3].

At high temperatures (800–900 K), Pt clusters remain essentially uncovered during CO oxidation and turnover rates become proportional to O_2 pressure and insensitive to CO pressure [11]:

$$r_{CO} = K_{O_2} k_O [O_2] = k_{eff} [O_2] \quad (2)$$

as first proposed by Langmuir [12] on bare Pt wires at high temperatures. In this kinetic regime, O_2 dissociation on bare Pt clusters limits CO oxidation rates and measured rate constants (k_{eff}) reflect the product of the equilibrium constant for molecular O_2 adsorption (K_{O_2}) to form O_2^* and its dissociation rate constant (k_O) on essentially bare Pt clusters. Their product, as it appears in k_{eff}, reflects differences in enthalpy (and entropy) between O_2(g) and the transition state that mediates O_2 dissociation elementary steps on such surfaces. O_2 dissociation is essentially barrierless (<3 kJ mol^{-1}) on bare surfaces and independent of the coordination of exposed atoms [13], as expected for the early nature of the transition states involved in these very exothermic steps; such transition states exhibit little if any product character and cannot sense changes in O* binding energy caused by concomitant changes in the size of metal cluster or in the average coordination of metal atoms exposed at their surfaces. As in the case of CO*-covered surfaces at low temperatures, CO oxidation turnover rates and activation barriers are insensitive to cluster size at high temperatures [13], albeit for mechanistic reasons that differ markedly in these two extreme kinetic regimes.

The mechanism and site requirements for catalytic CO oxidation on Pt at intermediate temperatures remain unclear and reported rate equations differ significantly among several studies. Rates are proportional to O_2 pressures in most of the studies reported, but kinetic orders in CO range from −0.3 (Pt supported on fiber glass; 475–650 K; [14]), to −0.5 (Pt monolith; 475–650 K; [15]) and even −1 (Pt(100) single-crystal; above 550 K; [8]).

Here, we report CO turnover rates measured under conditions of strict kinetic control on Pt clusters (1.8–25 nm mean cluster diameter) in this intermediate temperature range (723–793 K) and interpret the observed kinetic response and effects of cluster size in mechanistic terms. Measured turnover rates are consistent with kinetically-relevant O_2 dissociation on cluster surfaces partially covered by CO*. The rate constants for these O_2 dissociation steps are much smaller on small than on large Pt clusters, but without concomitant changes in measured CO adsorption equilibrium constants. We conclude that small clusters retain a smaller fraction of their exposed atoms available during catalysis than larger clusters, but that these active regions, residing at low-index planes with more highly coordinated exposed atoms, are similar in binding and reactivity on clusters of different size.

CO oxidation on Pt clusters occurs predominantly on low-index planes, which are more prevalent on larger clusters, because low-coordination sites, such as corners and edges, become decorated by strongly-bound and less reactive chemisorbed oxygen atoms. Such phenomena, often cited without direct evidence to account for cluster size effects, are shown here to account for the similar binding of CO* species on clusters that differ in size (1.8–25 nm) and in CO oxidation turnover rates. Residual undecorated surface regions account for the observed CO oxidation reactivity; these regions consist of low-index planes, where O* and CO* bind more weakly than on Pt atoms with lower coordination at corners and edges.

2. Experimental methods

2.1. Catalysts synthesis procedures

Supported Pt catalysts (0.2–0.5% wt.) were prepared by incipient wetness impregnation of SiO_2 (Davisil LS150A, Grace Davison; 100–150 μm; 340 m^2 g^{-1}) with aqueous hexachloroplatinic acid ($H_2PtCl_6(H_2O)_6$, Aldrich, CAS #16941-12-1). Silica supports were treated in flowing dry air (Praxair, 99.99%, 0.8 cm^3 g^{-1} s^{-1}) by heating at 0.083 K s^{-1} to 1073 K and holding for 3 h before contacting SiO_2 powders with the impregnating solutions. After impregnation, samples were treated overnight at 373 K in stagnant ambient air and individual portions were treated in flowing dry air (Praxair, 99.99%, 0.8 cm^3 g^{-1} s^{-1}) to different temperatures (823–973 K; 0.083 K s^{-1}) for 5 h; the intention and the observed effects of these treatments was to vary the Pt dispersion and cluster size over a range that is expected to cause significant changes in the coordination of exposed metal atoms (1.8–25 nm). Samples were then cooled to ambient temperature in flowing dry air, flushed with He, and exposed to 10% H_2/Ar (Praxair, certified standard, 0.8 cm^3 g^{-1} s^{-1}) by heating to 823 K (at 0.083 K s^{-1}) and holding for 3 h. This treatment was followed by cooling in He (Praxair UHP grade, 0.8 cm^3 g^{-1} s^{-1}) to ambient temperature and exposing samples to 1% O_2–He flow (Praxair certified standard, 0.8 cm^3 g^{-1} s^{-1}) for 4 h to passivate cluster surfaces before exposure to ambient air.

The number of Pt atoms exposed at cluster surfaces was measured from volumetric uptakes of strongly chemisorbed H_2 at 313 K (Quantasorb Chemisorption Analyzer; Quantachrome Corp.) by extrapolating isotherms (1–50 kPa H_2 pressure) to zero H_2 pressures, as reported elsewhere [16]. Mean cluster diameters were estimated from dispersion values by assuming hemispherical clusters with the bulk density of Pt metal (21.5 g cm^3; [17]).

2.2. Turnover rate and selectivity measurements

Catalytic CO oxidation rates were measured at 453–793 K using a quartz tube (8.1 mm inner diameter) with a K-type thermocouple at its external wall. Catalysts (0.2–0.5% wt. Pt/SiO_2) were diluted with inert SiO_2 (Davisil LS150A) to form mixtures with SiO_2/catalyst intraparticle mass ratios (λ) of 100–300 and then pelleted and sieved to retain 100–250 μm aggregates. These aggregates were then diluted with acid-washed quartz granules (100–250 μm, Fluka, #84880) at quartz/catalyst mass ratios (α) of 8000–30,000. Before dilution, SiO_2 (Davisil LS150A) and acid-washed quartz (Fluka) diluents were treated in dry air (Praxair, 99.99%, 0.8 cm^3 g^{-1} s^{-1}) at 1123 K (for 5 h) and 1173 K (for 2 h), respectively. Diluents alone were tested at the conditions of catalytic measurements and did not show detectable reaction rates.

Reactants were metered using electronic flow controllers (Porter, type 201) using 1% CO/He (Praxair certified standard), 5% O_2/He (Praxair certified standard), 1% O_2/He (Praxair certified standard), O_2 (Praxair UHP grade), and He (Praxair UHP grade). Samples were treated in 5% H_2/He (Praxair UHP grade; 1.67 cm^3 s^{-1}) by heating to 773 K at 0.083 K s^{-1} and holding for 600 s before rate measurements, and the lines were purged with He before introducing reactants. Reactant and product concentrations were measured using an Agilent 3000A Micro GC equipped with Poraplot Q and Mol Sieve 5A columns and thermal conductivity detectors.

2.3. Isotopic exchange measurements

$^{16}O_2$–$^{18}O_2$ exchange rates were measured using the same reaction system and treatment protocols as in the case of CO–O_2 reactions. A mixture of 5% $^{18}O_2$/He (Isotec, 97% at. ^{18}O) was used to carry out CO–$^{16}O_2$–$^{18}O_2$ and $^{16}O_2$–$^{18}O_2$ reaction experiments. The concentrations of the various dioxygen and carbon dioxide isotopologues

($^{16}O_2$, $^{16}O^{18}O$, $^{18}O_2$, $C^{16}O_2$, $C^{18}O_2$) were measured with a mass selective detector (Agilent 5973) without chromatographic separation.

3. Results and discussion

3.1. Exclusion of intraparticle and interparticle transport artifacts

Turnover rates of rigorous chemical origins require the strict absence of transport artifacts [18,19]. CO oxidation is prone to such artifacts because of its very exothermic nature ($\Delta H^0_{298} = -284$ kJ (mol CO)$^{-1}$ [20]) and because reaction rates increase as CO concentrations are depleted along the bed or within diffusion-limited catalyst pellets. These characteristics of CO oxidation catalysis lead to ubiquitous gradients in concentration and temperature within pellets and packed beds. Such gradients can be avoided by intrapellet and bed dilution with inert solids; rates that do not depend on the extent of dilution provide the only rigorous arbiter of the absence of non-chemical corruptions of measured rates [18,19].

The effects of intraparticle SiO_2/catalyst dilution ratios (λ = 100–300) and interparticle quartz/catalyst dilution ratios (α = 8000–30,000) on CO oxidation turnover rates are shown in Fig. 1 (0.5% wt. Pt/SiO_2, 3.3 nm clusters; 773 K; 0.01–0.15 kPa O_2 and 0.8 kPa CO). CO turnover rates did not depend on intraparticle or interparticle dilution ratios in this range, indicating that these dilution ratios lead to local concentrations and temperatures identical to those measured in the fluid phase. We conclude that rates on catalyst beds with λ values of 100–300 and α values of 8000–30,000 reflect the dynamics of the chemical reactions on Pt cluster surfaces without corrupting effects of mass or heat transfer at all conditions used in this study. Such dilution ratios, however, have seldom been used in previous studies, raising concerns about the chemical origins of such rate data and suggesting a plausible root cause for the previous contradictory rate data.

3.2. Kinetic dependence of CO oxidation turnover rates on reactant concentrations

The effects of O_2 and CO pressures on CO oxidation turnover rates were measured at 723–793 K (0.2–0.5% wt. Pt/SiO_2, 0.2–0.9 kPa CO; 0.01–0.4 kPa O_2). At CO pressures below 0.6 kPa, O_2 conversions were above 20%; these latter data were treated using mathematical formalisms for integral plug-flow reactors using a functional form of the rate equation inferred as an initial choice from low-conversion data. All rate data were then regressed to this functional form to estimate the kinetic and thermodynamic parameters in the rate equation and to assess the appropriateness of the sequence of elementary steps used to derive this rate equation (Section 3.3).

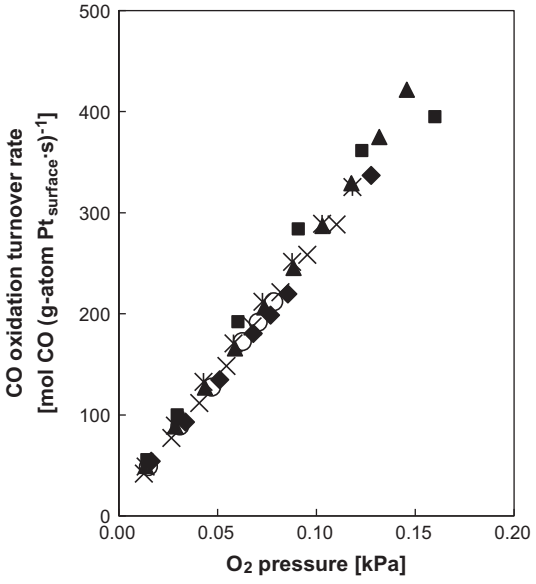

Fig. 1. Effects of intraparticle and interparticle mass dilution ratios on CO oxidation turnover rates (r_{CO}) on 0.5% wt. Pt/SiO_2 (3.3 nm mean cluster diameter; 773 K; 100 (▲), 200 (⨯, ■, ○, ♦) and 300 (×) intraparticle SiO_2/catalyst dilution ratios (λ); 8000 (▲, ⨯, ×), 10,000 (■), 15,000 (○) and 30,000 (♦) interparticle quartz/catalyst dilution ratios (α); 0.8 kPa CO).

Figs. 2 and 3 show the effects of O_2 (0.01–0.15 kPa; (a)) and CO (0.4–0.9 kPa (b)) pressures on CO oxidation turnover rates on 0.5% wt. Pt/SiO_2 (3.3 nm and 25 nm clusters) at 773 K. CO turnover rates were proportional to O_2 pressure and inhibited by CO; thus, mean reactant pressures ($[O_2]_{mean}$, $[CO]_{mean}$) are reported as the linear average of the inlet ($[O_2]_{inlet}$) and outlet ($[O_2]_{outlet}$) O_2 pressures:

$$[O_2]_{mean} = \left(\frac{[O_2]_{inlet} + [O_2]_{outlet}}{2}\right) \quad (3)$$

and as the average of the inverse pressure at the inlet ($[CO]^{-1}_{inlet}$) and the outlet ($[CO]^{-1}_{outlet}$) CO pressures:

$$[CO]_{mean} = \left(\frac{2}{1/[CO]_{inlet} + 1/[CO]_{outlet}}\right) \quad (4)$$

a choice made on the basis of the observed kinetic dependence for low-conversion data, for which averaging is made unnecessary by the differential nature of the packed bed reactor.

Fig. 4 shows inverse CO oxidation turnover rates on Pt (0.5% wt. Pt/SiO_2; 3.3 nm mean cluster diameter) as a function of the mean CO pressure. CO oxidation turnover rates show an apparent negative order in CO (−0.3 to −0.2); the reciprocal turnover rates shown in Fig. 4 have an apparent non-zero intercept. The same kinetic dependence on O_2 and CO was found on all Pt catalysts in this study and also throughout the entire temperature range (0.2–0.5% wt. Pt/SiO_2, 1.8–8.5 nm clusters; 723–793 K; see Supplementary Information, Section S1 for CO turnover rates as a function of O_2 or CO pressures). These data indicate that mechanistic interpretations of these data remain valid for all temperatures and cluster sizes used in this study; the fractional CO kinetic orders also indicate that surfaces are neither bare nor saturated with chemisorbed CO during catalysis, but exhibit intermediate CO* coverages in these experiments.

Previous studies at lower temperatures (360–473 K) showed that CO oxidation rates on CO-saturated Pt surfaces are proportional to O_2/CO ratios [3]. On the other hand, at very high temperatures (>800 K), O_2 activation occurs on essentially bare Pt clusters at rates that are proportional to O_2 pressure but insensitive to CO pressure [11]. At the intermediate temperatures used here (723–793 K), CO turnover rates seem to be consistent with Pt surfaces partially covered by CO*, on which inhibition by CO remains important, but vacancy sites (∗) become more abundant than at lower temperatures, as expected from the exothermic nature of CO adsorption processes. The inhibition by CO may reflect the presence of CO* or CO-derived species (C*, O*) at sites that would otherwise remain available for O_2 activation steps. These inhibition effects are fully reversible and deactivation or slow transients were not detected throughout this study; thus, even though CO* dissociation to form C* and O* species may indeed occur, it is a reversible step (and therefore quasi-equilibrated at the steady state of the overall catalytic sequence, since C* can only be removed by the microscopic reverse of CO* dissociation).

These data are consistent with a sequence of elementary steps (Scheme 1) in which O_2 absorbs molecularly via quasi-equilibrated steps (step 1, Scheme 1) and then dissociates via interactions with a vicinal vacant site (∗) (step 2, Scheme 1). O_2^* dissociation assisted by CO*, as observed at low temperatures (360–473 K, [3]), was also

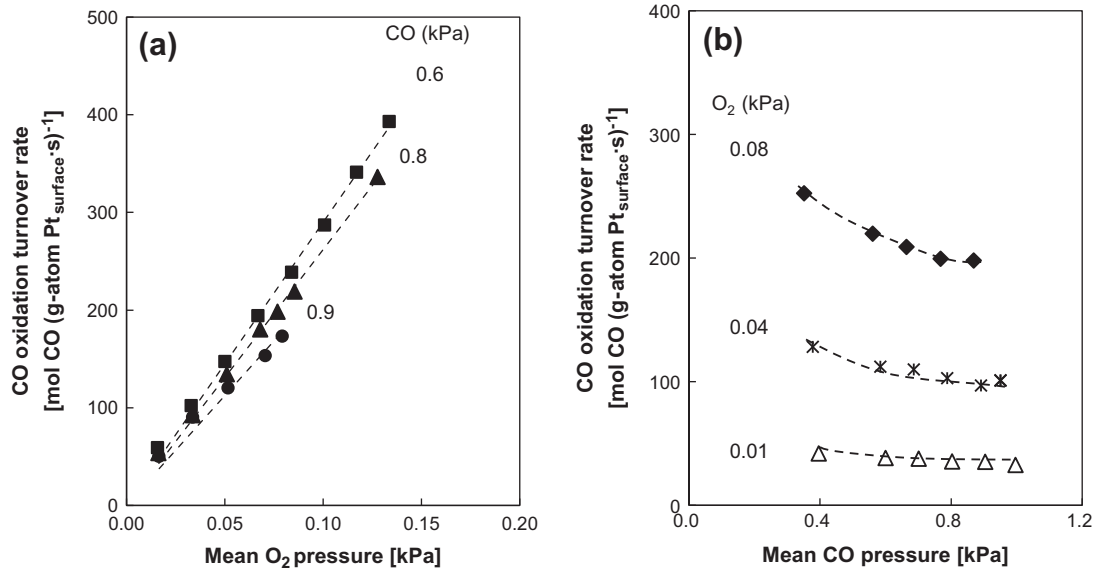

Fig. 2. Effects of O_2 (a) and CO (b) pressures on CO oxidation turnover rates (r_{CO}) on 0.5% wt. Pt/SiO_2 (3.3 nm mean cluster diameter; 773 K; 300 intraparticle SiO_2/catalyst ratio (λ); 8000 interparticle quartz/catalyst ratio (α); 1.8×10^8 cm^3 (STP) g^{-1} h^{-1}).

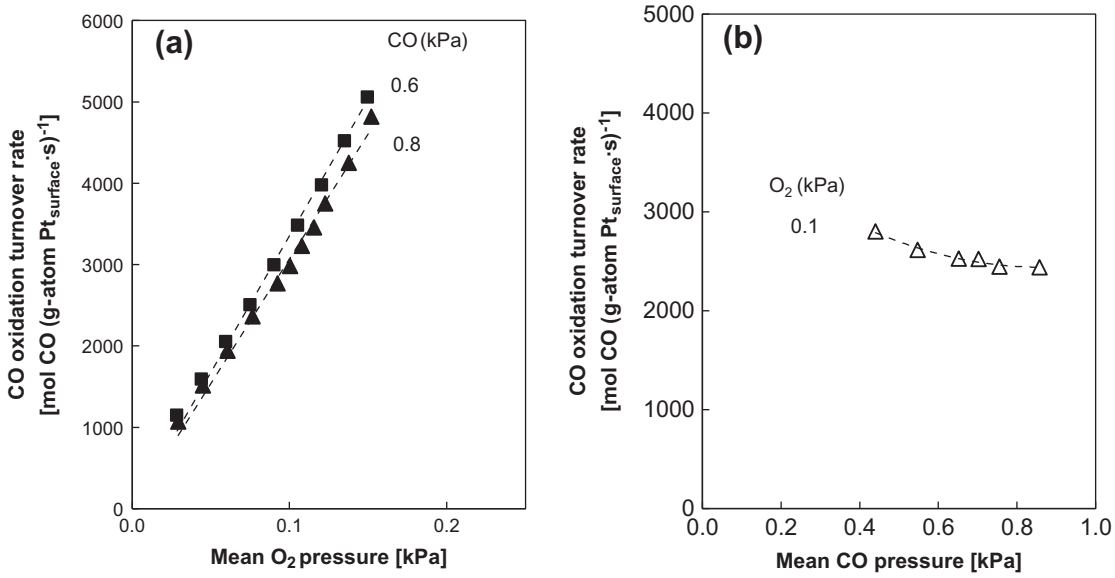

Fig. 3. Effects of O_2 (a) and CO (b) pressures on CO oxidation turnover rates (r_{CO}) on 0.5% wt. Pt/SiO_2 (25 nm mean cluster diameter; 773 K; 300 intraparticle SiO_2/catalyst ratio (λ); 8000 interparticle quartz/catalyst ratio (α); 1.8×10^8 cm^3 (STP) g^{-1} h^{-1}).

considered in an alternate pathway (step 2′, Scheme 1) but led to a rate equation that did not accurately describe the data at low CO pressures (Section 3.3; Supplementary Information, Fig. S9); at the intermediate CO* coverages prevalent at these temperatures (723–793 K), O_2^* dissociation occurs preferentially on vacancy sites, without the assistance by CO* that is required on surfaces saturated with CO* and largely devoid of vacant sites.

CO adsorbs molecularly on Pt (step 3, Scheme 1) in quasi-equilibrated steps and then reacts with O* to form CO_2 (step 5, Scheme 1); CO can also dissociate (step 4, Scheme 1) to form C* and O*. In this scheme, the kinetic coupling of O_2 activation with the step that removes O* via its reaction with CO* (step 5, Scheme 1) determines the O* coverages prevalent during steady-state CO oxidation catalysis. C* coverages are determined by the coupling of the C* formation step (forward step 4, Scheme 1) and C* removal by O* (reverse step 4, Scheme 1); the absence of any other routes for C* removal leads to the equilibration of the forward and reverse steps for CO* dissociation (step 4). The desorption of the CO_2 molecules formed in step 5 (step 6, Scheme 1) then completes a catalytic turnover. An alternate route in which CO_2 forms via CO* activation assisted by a vicinal CO* to also form C* (which later reacts with O*) has been previously proposed as a minority route at very low temperatures (<500 K) and O_2/CO ratios <100 [10], but it would not describe the observed kinetic dependence on O_2 pressure (Figs. 2 and 3); the co-existence of both routes for CO_2 formation (CO* + O* and CO*+CO*) would lead to a non-zero intercept of the CO oxidation turnover rates as a function of the O_2 pressure, in contradiction with the data shown in Figs. 2 and 3.

Next, we derive the functional form of the CO oxidation rates from these elementary steps and concomitant assumptions about

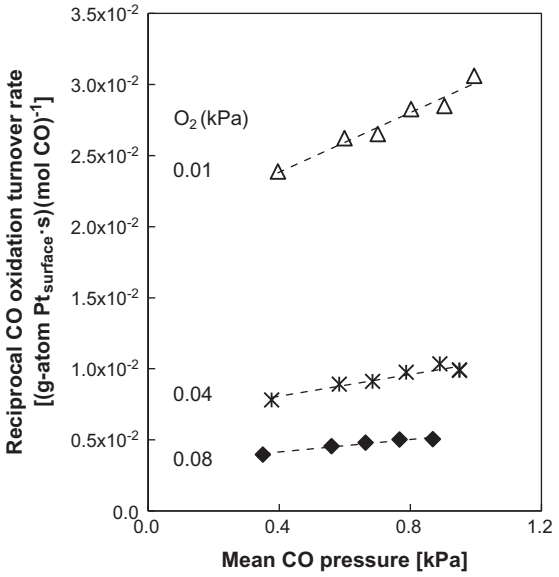

Fig. 4. Effects of CO pressure on the reciprocal CO oxidation turnover rates ($1/r_{CO}$) on 0.5% wt. Pt/SiO_2 (3.3 nm mean cluster diameter; 773 K; 300 intraparticle SiO_2/catalyst ratio (λ); 8000 interparticle quartz/catalyst ratio (α); 1.8×10^8 cm^3 (STP) g^{-1} h^{-1}).

their reversibility and show that the resulting rate equation accurately describes measured rates and is also consistent with independent mechanistic probes based on isotopic exchange.

3.3. Kinetic analysis of the sequence of elementary steps

A CO oxidation rate equation can be derived from the elementary steps in Scheme 1 by applying the pseudo-steady-state and equilibrium assumptions and considering (∗), (O*), (CO*) and (C*) as the most abundant surface intermediates (MASI). The rate of step 5 (Scheme 1) gives the CO oxidation turnover rate (r_{CO}) at steady state in terms of the concentration of O* and unoccupied sites (∗):

$$r_{CO} = 2K_{CO}k_{CO-O}[CO][O^*][*] \quad (5)$$

In this equation, K_{CO} is the equilibrium constant for molecular CO adsorption and k_{CO-O} is the rate constant for O* reactions with CO*. The pseudo-steady-state concentration of [O*] for reversible O_2^* dissociation (step 2, Scheme 1) is given by:

$$[O^*] = \frac{2K_{CO}k_{CO-O}[CO]}{k_{Or}}\left(\frac{1}{2}\left(\sqrt{1+\frac{K_{O_2}k_{Of}k_{Or}}{(K_{CO}k_{CO-O})^2}\frac{[O_2]}{[CO]^2}}-1\right)\right)[*] \quad (6)$$

Here, K_{O_2} is the equilibrium constant for molecular O_2 adsorption and k_{Of} and k_{Or} are the forward and reverse rate constants for O_2^* dissociation, respectively.

The term in parenthesis in Eq. (6) is denoted as χ in what follows. The value of χ reflects the ratio of the rate at which O* recombines to re-form O_2 (r_{Or}, reverse step 2, Scheme 1) to that at which O* reacts with CO* to form CO_2 (r_{CO}, step 5, Scheme 1):

$$\chi = \frac{r_{Or}}{r_{CO}} = \frac{k_{Or}[O^*]^2}{2K_{CO}k_{CO-O}[CO][O^*][*]} = \frac{1}{2}\left(\sqrt{1+\frac{K_{O_2}k_{Of}k_{Or}}{(K_{CO}k_{CO-O})^2}\frac{[O_2]}{[CO]^2}}-1\right) \quad (7)$$

As a result, this equation provides a rigorous measure of the reversibility of O_2 dissociation steps during CO oxidation catalysis. Values of $\chi \ll 1$ reflect irreversible O_2^* dissociation, while $\chi \gg 1$ indicates that O_2^* dissociation and O* recombination steps are in quasi-equilibrium. These equations, together with a site balance:

$$[*] + [O^*] + [CO^*] + [C^*] = [L] \quad (8)$$

in which [L] is the total number of sites, taken here as the number of exposed Pt atoms at cluster surfaces, and the equilibrium assumptions for CO* and C* lead to a general equation for CO oxidation turnover rates (per exposed metal atom; details of the derivation in Supplementary Information, Section S2):

$$r_{CO} = \frac{\frac{2(K_{CO}k_{CO-O})^2[CO]^2}{k_{Or}}(\chi)}{\left(1+K_{CO}[CO]+\frac{2K_{CO}k_{CO-O}[CO]}{k_{Or}}(\chi)+\frac{K_C k_{or}}{2k_{CO-O}(\chi)}\right)^2} \quad (9)$$

$$\uparrow\ [*] \quad \uparrow\ [CO*] \quad \uparrow\ [O*] \quad \uparrow\ [C*]$$

where K_C is the equilibrium constant for CO dissociation (step 4, Scheme 1). The denominator terms labeled as [∗], [O*], [CO*], and

	Elementary Step	Kinetic/Thermodynamic Constant
1	$O_2 + * \rightleftharpoons O_2*$	K_{O_2}
2	$O_2* + * \rightleftarrows 2O*$	k_{Of}, k_{Or}
2'	$O_2* + CO* \rightarrow CO_2* + O*$	k_{O_2*-CO*}
3	$CO + * \rightleftharpoons CO*$	K_{CO}
4	$CO* + * \rightleftharpoons C* + O*$	K_C
5	$CO* + O* \rightarrow CO_2* + *$	$k_{CO\text{-}O}$
6	$CO_2* \rightarrow CO_2 + *$	k_{CO_2}
7[a]	$^iO_2* + {}^jO* \rightarrow {}^iO* + {}^iO^jO*$ [b]	$k_{O\text{-}ex}$

* refers to an unoccupied Pt surface atom; ⇌ denotes a quasi-equilibrated step and ⟶ an irreversible step; f: forward; r: reverse. [a] Considered during $^{18}O_2$-$^{16}O_2$ exchange reactions; [b] i and j are used to differentiate the oxygen atoms

Scheme 1. Proposed sequence of elementary steps and associated kinetic or thermodynamic constants during CO oxidation reactions on Pt clusters.

Table 1
χ and η parameters on 0.5% wt. Pt/SiO_2 (3.3 and 25 nm mean cluster diameter) at 773 K.

Mean Pt cluster size (nm)	χ[a]	η[b]
3.3	0.012 ± 0.008	0.30 ± 0.02
25	0.02 ± 0.01	0.20 ± 0.01

(0.8 kPa CO; 0.7 kPa O_2; 773 K).

[a] $\chi = r_{Or}/r_{CO}$; ratio of the rate at which O* recombines to re-form O_2 (r_{Or}) to that at which O* reacts with CO* to form CO_2 (r_{co}) (Eq. (7); Section 3.3). Obtained from the fitting of the kinetic data to the functional form of Eq. (9).

[b] $\eta = r_{ex,ss}/r_{ex,eq}$; ratio between $^{16}O_2$–$^{18}O_2$ isotopic exchange rate during CO–$^{16}O_2$–$^{18}O_2$ ($r_{ex,ss}$; steady state) and $^{16}O_2$–$^{18}O_2$ ($r_{ex,eq}$; equilibrium) mixtures (Eq. (15); Section 3.5).

[C*] represent their respective coverages during catalysis (relative to [∗]).

The regression of all rate data to the functional form of Eq. (9) by minimization of residuals (Supplementary Information, Section S3 for method details) led to χ values (Eq. (7)) of 0.04–2.0 × 10^{-3} (0.5% wt. Pt/SiO_2; 3.3 nm mean cluster diameter; 773 K; 0.2–0.9 kPa CO; 0.01–0.4 kPa O_2; Table 1 for χ values for 3.3 and 25 nm Pt clusters), indicating that O_2^* dissociation is essentially irreversible. Small values of χ lead to the asymptotic form of Eq. (9) for irreversible O_2^* dissociation (step 2, Scheme 1) ($\chi \ll 1$) (Supplementary Information, Section S2 for details in the derivation of the rate equation):

$$r_{CO} = \frac{K_{O_2}k_{Of}[O_2]}{\left(1 + K_{CO}[CO] + \frac{K_{O_2}k_{Of}}{2K_{CO}k_{CO-O}}\frac{[O_2]}{[CO]} + \frac{2K_C K_{CO}^2 k_{CO-O}}{K_{O_2}k_{Of}}\frac{[CO]^2}{[O_2]}\right)^2} \quad (10)$$

($[*]$, $[CO*]$, $[O*]$, $[C*]$)

where the O* coverage (Eq. (6)) is now given by:

$$[O^*] = \frac{1}{2}\frac{K_{O_2}k_{Of}}{K_{CO}k_{CO-O}}\frac{[O_2]}{[CO]}[*] \quad (11)$$

The values of these groupings of kinetic and thermodynamic parameters ($K_{O_2}k_{Of}$, K_{CO}, $K_{O_2}k_{Of}/(2K_{CO}k_{CO-O})$ and $2K_C K_{CO}^2 k_{CO-O}/(K_{O_2}k_{Of})$) were determined by regression of all rate data to the functional form of Eq. (10) (0.2–0.9 kPa CO; 0.01–0.4 kPa O_2) at 773 K (Table 2 at 773 K, 1.8–25 nm clusters; parity plots relating measured and predicted rates in Fig. 5a and in Fig. S7 in the Supplementary Information). We have used this function within the formalism of integral plug-flow reactors (procedure shown in Supplementary Information, Section S4). The [O*] and [C*] terms in the denominator of Eq. (10) are much smaller than those for [∗] and [CO*]; they remain below 0.04 and 0.002 fractional coverages, respectively, at all conditions used here (0.2–0.5% wt. Pt/SiO_2; 723–793 K; 0.2–0.9 kPa CO; 0.01–0.4 kPa O_2). With (∗) and (CO*) as MASI, Eq. (10) becomes:

$$r_{CO} = \frac{K_{O_2}k_{Of}[O_2]}{(1 + K_{CO}[CO])^2} \quad (12)$$

($[*]$, $[CO*]$)

Eq. (12) describes all rate data with the same accuracy as the full form of Eq. (10), as shown by the parity plots for measured and predicted CO turnover rates (Figs. 5b and 6 at 773 K for 3.3 nm and 25 nm clusters, respectively; Fig. 7 at 723–793 K for 3.3 nm clusters; Fig. S8 in Supplementary Information at 773 K for 1.8–8.5 nm clusters). The values of K_{CO} at 773 K (0.75 kPa^{-1}, Table 2) indicate that fractional CO* coverages are 0.41 on Pt clusters (3.3 nm and 25 nm, 0.5% wt. Pt/SiO_2; 0.01–0.4 kPa O_2) at the highest CO pressure (0.9 kPa) used in these experiments. The $K_{O_2}k_{Of}$ term in Eq. (12) reflects the sum of the activation barrier for O_2^* dissociation (step 2, Scheme 1) and the (negative) enthalpy of O_2 molecular adsorption (step 1, Scheme 1). The effects of temperature on $K_{O_2}k_{Of}$ and K_{CO} (Fig. 8) are consistent with the expected values of O_2 dissociation barriers and CO adsorption enthalpies at low CO* coverages, as we discuss in detail in the next section.

We also examined the possible alternate route in which O_2^* dissociation is assisted by CO* (step 2′, Scheme 1) [3]. In this case, turnover rates are given by the net rate of step 2′ (Scheme 1) and lead to the rate equation:

$$r_{CO} = \frac{K_{CO}K_{O_2}k_{O_2*-CO*}[O_2][CO]}{(1 + K_{CO}[CO])^2} \quad (13)$$

($[*]$, $[CO*]$)

with (∗) and (CO*) as MASI. Here, k_{O_2*-CO*} is the rate constant for CO*-assisted O_2^* dissociation on CO-covered sites. The parity plot for measured and predicted CO turnover rates (Fig. S9 in Supplementary Information, 0.5% wt. Pt/SiO_2, 3.3 nm clusters, 773 K) shows that Eq. (13) fails to describe the rate data at low CO pressures and describes the rest of the rate data less accurately than Eq. (12).

3.4. Temperature dependence of rate and equilibrium constants

The kinetic and thermodynamic parameters in Eq. (12) ($K_{O_2}k_{Of}$ and K_{CO}) were estimated at temperatures between 723 K and 793 K (0.2–0.9 kPa CO; 0.01–0.4 kPa O_2; 0.5% wt. Pt/SiO_2; 3.3 nm mean cluster diameter) by regression of all rate data to the functional form of Eq. (12). The parity plots in Fig. 7 show that this rate equation accurately describes all rate data.

Arrhenius plots for the equilibrium and rate constants for (a) O_2 activation and (b) for CO adsorption on Pt (0.5% wt. Pt/SiO_2; 3.3 nm mean cluster size) are shown in Fig. 8. The measured barrier for O_2 activation (E_{O_2}, from $K_{O_2}k_{Of}$ data in Fig. 8a) is 8 ± 2 kJ mol^{-1} and is given by:

$$E_{O_2} = E_{2f} + \Delta H_{O_2} \quad (14)$$

and reflects the enthalpy differences between the O_2 dissociation transition state and an O_2(g) molecule, given by the sum of the activation barrier for O_2^* dissociation (E_{2f}; step 2, Scheme 1) and the (negative) enthalpy of molecular adsorption of O_2 (ΔH_{O_2}; step 1, Scheme 1). The measured effective barrier for O_2 activation (8 ± 2 kJ mol^{-1}) on Pt (0.5% wt. Pt/SiO_2; 3.3 nm mean cluster size) is very similar to the values derived from DFT treatments on bare Pt(1 1 1) surfaces (10 kJ mol^{-1} [21]) and Pt clusters (<20 kJ mol^{-1} site average, 201 Pt atoms, 1.8 nm cluster diameter [13]) and on Pt(1 1 1) surfaces partially covered with CO* (32 kJ mol^{-1}, 0.44 fractional CO* coverage [22]).

The CO adsorption enthalpy (from K_{CO}, Fig. 8b) was −108 ± 7 kJ mol^{-1} on Pt (0.5% wt. Pt/SiO_2; 3.3 nm mean cluster size). These values are in reasonable agreement with those measured by calorimetry at 0.3–0.4 fractional CO* coverages (−150 kJ mol^{-1} on Pt(1 1 0) [23]; −118 kJ mol^{-1} on Pt(1 1 1) [24]; −140 kJ mol^{-1} on Pt/SiO_2 with Pt clusters between 2–5 nm [25]) and with DFT-derived enthalpies on bare and CO*-saturated Pt clusters (−120 kJ mol^{-1} on Pt(1 1 1) terrace sites, −162 kJ mol^{-1} edges and 171 kJ mol^{-1} on corners at zero coverage; −79 kJ mol^{-1} on Pt(1 1 1) terrace sites, −129 kJ mol^{-1} edges and 143 kJ mol^{-1} on corners at CO-saturation coverages; 201 Pt atoms; 1.8 nm mean cluster size [3]). These 3.3 nm Pt clusters are expected to expose surfaces with 20–30% of atoms at corner or edge sites (considering several possible cluster shapes [27]), yet their CO adsorption enthalpies measured during CO oxidation are similar (and even less negative) that those typical of low-index planes, suggesting

Table 2
Rate and equilibrium parameters for CO–O_2 reactions (Eq. (10)) on 0.2–0.5% wt. Pt/SiO_2 (1.8–25 nm mean cluster diameter) at 773 K.

Mean Pt cluster size (nm)	Parameter[a]			
	$K_{O_2}k_{Of}$ (kPa^{-1} s^{-1})	K_{CO} (kPa^{-1})	$\frac{K_{O_2}k_{Of}}{2K_{CO}k_{CO-O}}$ (–)	$\frac{2K_C K_{CO}^2 k_{CO-O}}{K_{O_2}k_{Of}}$ (kPa^{-1})
1.8	4500 ± 300	0.67 ± 0.05	0.10 ± 0.09	$5 \times 10^{-4} \pm 3 \times 10^{-4}$
3.3	4700 ± 100	0.75 ± 0.02	0.06 ± 0.05	$3 \times 10^{-4} \pm 1 \times 10^{-4}$
4.3	7600 ± 200	0.88 ± 0.01	$1.0 \times 10^{-3} \pm 8 \times 10^{-4}$	0
8.5	31,000 ± 1000	0.70 ± 0.03	0.005 ± 0.003	$2 \times 10^{-5} \pm 1 \times 10^{-5}$
25	32,000 ± 500	0.6 ± 0.1	0.10 ± 0.05	$1.0 \times 10^{-5} \pm 0.9 \times 10^{-6}$

[a] Obtained from regression of the kinetic data to the functional form of Eq. (10) by minimization of the square of the residuals.

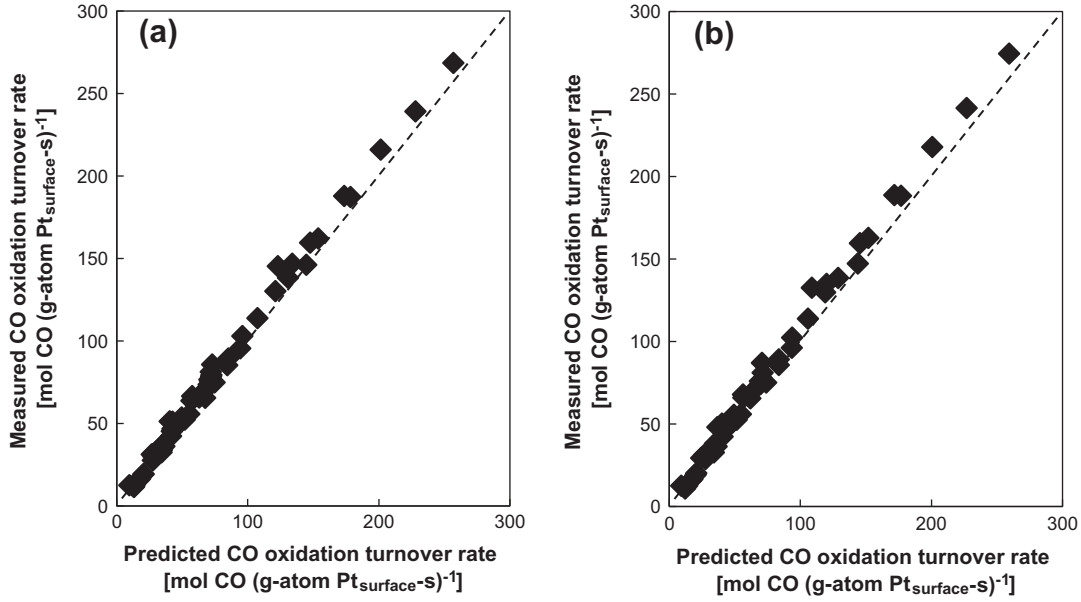

Fig. 5. Measured CO oxidation turnover rates (r_{CO}) on 0.5% wt. Pt/SiO_2 vs. predicted CO oxidation turnover rates using (a) the full form of the turnover rate expression (Eq. (10)) and (b) the simplified form by considering (∗) and (CO*) as the most abundant surface intermediates (Eq. (12)) (3.3 nm mean cluster diameter; 773 K; 300 intraparticle SiO_2/catalyst ratio (λ); 8000 interparticle quartz/catalyst ratio (α); 1.8×10^8 cm^3 (STP) g^{-1} h^{-1}).

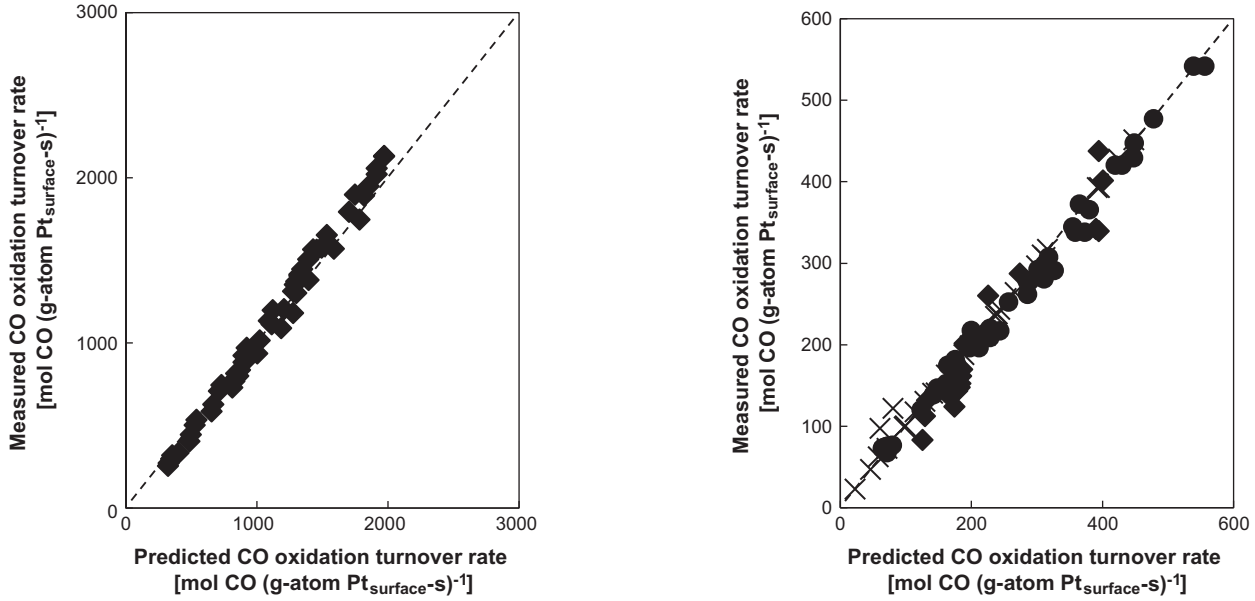

Fig. 6. Measured CO oxidation turnover rates (r_{CO}) on 0.5% wt. Pt/SiO_2 vs. predicted CO oxidation turnover rates using the simplified form of Eq. (10), considering (∗) and (CO*) as the most abundant surface intermediates (Eq. (12)) (25 nm mean cluster diameter; 773 K; 300 intraparticle SiO_2/catalyst ratio (λ); 8000 interparticle quartz/catalyst ratio (α); 1.8×10^8 cm^3 (STP) g^{-1} h^{-1}).

Fig. 7. Measured CO oxidation turnover rates (r_{CO}) on 0.5% wt. Pt/SiO_2 vs. predicted CO oxidation turnover rates using the simplified form of Eq. (10), considering (∗) and (CO*) as the most abundant surface intermediates (Eq. (12)), at 623 K (×), 748 K (●) and 793 K (♦) (3.3 nm mean cluster diameter; 300 intraparticle SiO_2/catalyst ratio (λ); 8000 interparticle quartz/catalyst ratio (α); 1.8×10^8 cm^3 (STP) g^{-1} h^{-1}).

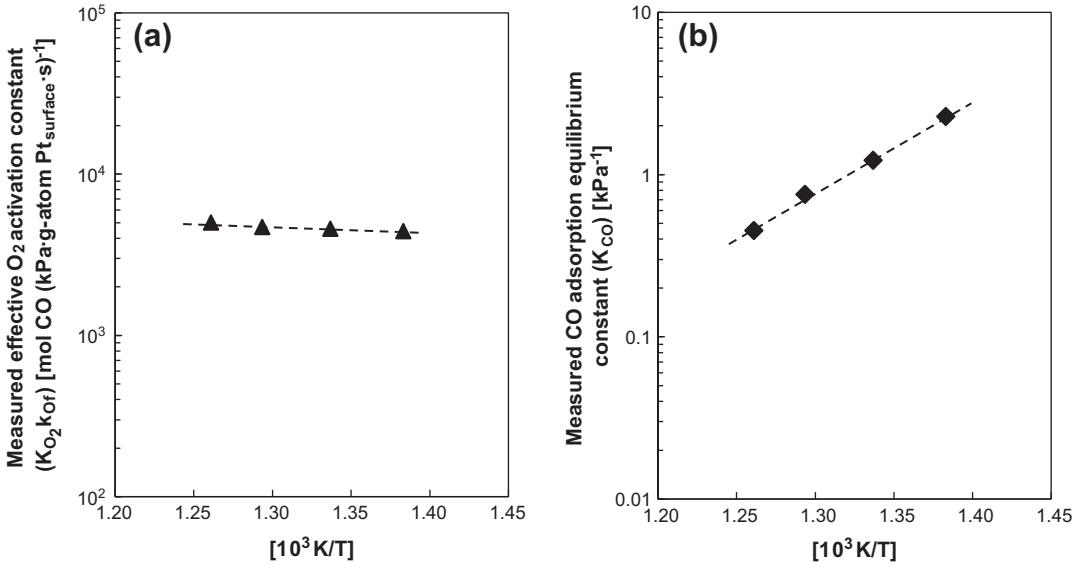

Fig. 8. Arrhenius plots of effective O_2 activation constant ((a); $K_{O_2}k_{Of}$) and CO adsorption equilibrium constant ((b); K_{CO}). (0.5% wt. Pt/SiO_2, 3.3 nm mean cluster diameter; 300 intraparticle SiO_2/catalyst ratio (λ); 8000 interparticle quartz/catalyst ratio (α); 0.2–0.9 kPa CO; 0.01–0.4 kPa O_2).

that the exposed atoms responsible for CO oxidation reside predominantly on planes exposing highly coordinated Pt atoms. These conclusions are confirmed in Sections 3.5 and 3.6 from the measured effects of cluster size on kinetic parameters and from $^{16}O_2$–$^{18}O_2$ isotopic exchange rates in the absence and presence of CO.

3.5. Isotopic assessment of O_2 activation steps

The irreversible nature of O_2 dissociation steps (step 2, Scheme 1) was probed by measuring $^{16}O_2$–$^{18}O_2$ isotopic exchange rates on Pt (0.5% wt. Pt/SiO_2; 3.3 nm mean cluster size; 773 K; 0.7 kPa total O_2 pressure; equimolar $^{16}O_2$–$^{18}O_2$ mixture) in the absence and presence of CO (0.8 kPa). $^{16}O_2$–$^{18}O_2$ exchange to form $^iO^jO^*$ (i, j = 18 or 16) proceeds via concerted reactions between $^iO_2^*$ and vicinal $^jO^*$ (step 7, Scheme 1), as observed from the oxygen kinetic dependence of ^{16}O–^{18}O rates on Pt clusters (0.2% wt. Pt/Al_2O_3, 1.8 and 8.5 nm clusters, equimolar $^{16}O_2$–$^{18}O_2$ mixtures [13,26]). Exchange rates are proportional to the surface coverages of $^iO_2^*$ and $^jO^*$, in which $^iO_2^*$ species are equilibrated with oxygen in the gas phase (step 1, Scheme 1) [13]. Thus, the ratios between $^{16}O_2$–$^{18}O_2$ isotopic exchange rate during CO–$^{16}O_2$–$^{18}O_2$ ($r_{ex,ss}$; steady state) and $^{16}O_2$–$^{18}O_2$ ($r_{ex,eq}$; equilibrium) mixtures (denoted here as η) can be expressed as:

$$\eta = \frac{r_{ex,ss}}{r_{ex,eq}} = \frac{k_{O\text{-}ex}([^iO_2^*][^jO^*])_{ss}}{k_{O\text{-}ex}([^iO_2^*][^jO^*])_{eq}} = \frac{O_2([O^*][*])_{ss}}{O_2([O^*][*])_{eq}} \quad (15)$$

where i and j denote 16 (or 18) and 18 (or 16), respectively, and $[O^*]$ is the combined $^{16}O^*$ and $^{18}O^*$ coverages. η reflects the O^* coverages during steady-state catalysis ($[O^*]_{ss}$) relative to those at equilibrium ($[O^*]_{eq}$), and consequently, the extent of O^* equilibration with O_2^* (step 2, Scheme 1) during CO–$^{16}O_2$–$^{18}O_2$ reactions. The O^* coverages during exchange with $^{18}O_2$–$^{16}O_2$ mixtures reflect those at equilibrium between O_2 and O^* ($[O^*]_{eq}$, steps 1 and 2 in Scheme 1) because in the absence of scavenging chemical reactions, O^* can only be removed by recombinative desorption:

$$[O^*]_{eq} = \sqrt{K_{O_2}K_O[O_2]}[*]_{eq} \quad (16)$$

where K_{O_2} and K_O are the equilibrium constants for molecular (step 1, Scheme 1) and dissociative O_2 adsorption (equilibrated step 2, Scheme 1). The O^* coverages during steady-state catalysis ($[O^*]_{ss}$) are given by the pseudo steady-state balance of O^* (Eq. (6), Section 3.3), which simplifies to Eq. (11) for irreversible O_2^* dissociation. Substituting Eqs. (11) and (16) into Eq. (15) gives η values as a function of rate and equilibrium constants:

$$\eta = \frac{\frac{K_{O_2}k_{Of}}{2K_{CO}k_{CO-O}}\frac{[O_2]}{[CO]}[*]_{ss}^2}{(\sqrt{K_{O_2}K_O[O_2]})[*]_{eq}^2} \quad (17)$$

A value of η near unity would reflect O^* coverages unperturbed by the presence of CO (which scavenges O^* via step 5 in Scheme 1), which would indicate that O^* remains in equilibrium with O_2(g) during CO oxidation.

These ratios (η) were compared with χ values obtained from the kinetic analysis of the sequence of elementary steps (Eq. (7), Section 3.3), since χ reflects the extent of O^* equilibration with O_2^* (step 2, Scheme 1) during CO oxidation. The values of η from isotopic exchange rates with and without CO (0.8 kPa CO; 0.7 kPa O_2; 0.5% wt. Pt/SiO_2, 3.3 nm clusters, 773 K) were much smaller than unity (η = 0.3), but significantly larger than χ values measured from rate data at the same conditions ($\chi = 4.3 \times 10^{-3}$ on 0.5% wt. Pt/SiO_2, 3.3 nm clusters, 773 K, 0.8 kPa CO, 0.7 kPa O_2). A χ value of 0.3, if correct, would not allow the accurate expansion of Eqs. (7) and (9) into their asymptotic form for irreversible oxygen activation (Eq. (10)), yet such an expansion led to an equation that accurately described all rate data (0.5% wt. Pt/SiO_2; 3.3 nm mean cluster diameter; 773 K, Figs. 5–7).

The term η (Eq. (15)) reflects O^* coverages during steady-state catalysis divided by those present if equilibrium with O_2(g) were to prevail during CO-O_2 reactions. The χ term (Eq. (7)) is the ratio of rates for O^* recombination (reverse step 2, Scheme 1) and O^* reactions with CO^* to form CO_2^* (step 5, Scheme 1); it reflects the extent of O^* equilibration with O_2(g) specifically at those sites where CO oxidation catalysis occurs. We conclude that η values (Eq. (15)) larger than measured χ values (Eq. (7)) must reflect the presence of O^* species that can exchange but do not readily react with CO^* during CO–$^{16}O_2$–$^{18}O_2$ reactions. Such species are plausibly considered to be strongly-bound O^* at low-coordination exposed Pt atoms (e.g., edges, corners, steps), which would react with CO^* more slowly than O^* species at sites with higher coordination prevalent in low-index planes. Density functional estimates

show that O* binds on corner and edges (383–410 kJ mol^{-1} bond energy) more strongly than on Pt(1 1 1) terraces (372–375 kJ mol) at low O* coverages on Pt clusters (201 atom cuboctahedral Pt cluster, 1.8 nm cluster diameter; [13]). These strongly-bound O* species are less reactive for H-abstraction from CH_4 [13] and C_2H_6 [26] than O* atoms at exposed low-index planes. O* species at low-coordination Pt atoms "decorate" such sites, rendering them unreactive for CO oxidation. Such decoration effects are consistent with CO adsorption enthalpies measured during CO oxidation catalysis (-108 ± 7 kJ mol^{-1} on 0.5% wt. Pt/SiO_2; 3.3 nm mean cluster size), which resemble those for low-index planes (-120 kJ mol^{-1} on Pt(1 1 1) terrace sites at zero coverages and -79 kJ mol^{-1} on Pt(1 1 1) terrace sites at CO-saturation coverages; 201 Pt atoms; 1.8 nm mean cluster size [3]). As we discuss below, these conclusions also account for the similar CO adsorption enthalpies measured during CO oxidation catalysis on large and small Pt clusters (Section 3.6).

The higher than expected observed $^{16}O_2$–$^{18}O_2$ exchange rates (and associated η) may reflect contributions from low-coordination Pt atoms that are decorated by O* species but do not contribute to CO–O_2 reaction turnovers. Such O* species would not lead to more reversible O_2 dissociation steps merely because of their strong binding. O* recombination steps are highly endothermic and their concomitant late transition states would make recombination barriers increase in concert with increasing O* binding energies as atoms with lower coordination become prevalent on small clusters. In contrast, O* reactions with CO* are exothermic reactions with earlier transition states than those for O* recombination and therefore the increase in barriers with the concomitant increase in the binding properties of adsorbed species involved as reactants (O* and CO*) is less pronounced than for O* recombination, making χ values (ratio of rates for O* recombination and O* reactions with CO* to form CO_2^*, Eq. (7)) actually be lower on corner and edge sites. The recombination of O* is not required, however, to form $^{16}O^{18}O$ from $^{16}O_2$–$^{18}O_2$ mixtures, because $^{16}O^{18}O$ can also form via concerted $^iO_2^*$ reactions with $^jO^*$ (step 7, Scheme 1; i, j = 18 or 16). The formation of $^{16}O^{18}O$ via $^iO_2^*$ reactions with $^jO^*$ is consistent with intrinsic barriers for O* recombination to form $^iO^jO^*$ that are much higher than those for $^iO^jO^*$ formation via concerted reactions of $^iO_2^*$ reactions with $^jO^*$ (200 kJ mol^{-1} vs. 27 kJ mol^{-1} for O* recombination and concerted reactions, respectively [13], DFT estimates on (1 1 1) facets of cuboctahedral 1.8 nm Pt clusters with 201 atoms). Thus, measured η values higher than χ reflect O* atoms on low-coordination Pt sites that are less perturbed by the presence of CO than O* on low-index planes, and consequently, O* coverages would be higher on corners and edges than on terrace sites.

Next, we examine the effects of the binding properties of Pt on O* coverages during CO–O_2 reactions by examining how changes in the binding properties of Pt caused by changes in Pt coordination would influence the apparent activation energies for the elementary steps that determine O* coverages. O* coverages during CO–O_2 reactions are determined by the kinetic coupling between O_2 activation that form O* (steps 1 and 2, Scheme 1) and CO oxidation by O* (step 5, Scheme 1) (Eq. (11)), which removes O*. For irreversible O_2^* dissociation, O* coverages are given by:

$$\frac{[O^*]}{[*]} = \frac{K_{O_2} k_{Of}}{2K_{CO} k_{CO-O}} \frac{[O_2]}{[CO]} = A \frac{\exp\left(-\frac{E_{O_2}}{RT}\right)}{\exp\left(-\frac{2E_{CO-O}}{RT}\right)} \frac{[O_2]}{[CO]} \quad (18)$$

The lumped kinetic and thermodynamic constants determine how binding properties influence O* coverages. E_{O_2} is the apparent activation energy for O_2 dissociation (defined in Eq. (14), Section 3.4), E_{CO-O} is the apparent activation energy for CO* reactions with O*, and A is an overall pre-exponential factor. The effective barrier for CO reactions with O* is given by the sum of the barriers for CO–O* reactions (E_5; forward step 5, Scheme 1) and the (negative) enthalpy of CO adsorption (ΔH_{CO}; step 3, Scheme 1):

$$E_{CO-O} = E_5 + \Delta H_{CO} \quad (19)$$

and reflects enthalpy differences between the CO oxidation transition state and a CO(g) molecule and an chemisorbed oxygen atom (O*). The E_{O_2} term in the numerator of Eq. (18) reflects the enthalpy differences between the O_2 dissociation transition state and an O_2(g) molecule, given by the sum of O_2^* dissociation barriers (E_{2f}; forward step 2, Scheme 1) and the (negative) enthalpy of molecular O_2 adsorption (ΔH_{O_2}; step 1, Scheme 1), as defined in Eq. (14). Thus, changes in the binding properties of Pt caused by changes in Pt coordination would influence O* coverages during CO–O_2 reactions via concomitant changes in the relative stability between O_2 dissociation transition states (steps 1 and 2; E_{O_2}) and those for CO reactions with O* (step 5; E_{CO-O}).

These relative stabilities depend, in turn, on the lateness of each transition state, which determine how the binding of reactants and products influence the stability of the transition state for the specific elementary state. O_2 dissociation (steps 1 and 2, Scheme 1) is very exothermic and proceeds via reactant-like early transition states; thus, the stronger binding of the products on low-coordination sites is largely inconsequential for activation barriers, as confirmed by DFT calculations on bare Pt clusters (1.8 nm cuboctahedral Pt cluster with 201 atoms [13]). O* reactions with CO* are also exothermic, but transition states occur later along the reaction coordinate than for O_2 activation and consequently exhibit a less reactant-like character. As a result, stronger binding of the adsorbed species involved as reactants (CO*, O* at low-coordination sites on smaller clusters) preferentially stabilizes reactants (O* and CO*) over CO*–O* transition states and lead to higher activation barriers for this step at low-coordination sites. DFT-derived activation energies (E_{CO-O}; Eq. (19)) on Pt clusters (201 atom cuboctahedral Pt cluster, 1.8 nm cluster diameter) indeed show higher values on Pt atoms with an average coordination number of 6.5 (by 15 kJ mol^{-1}) than on atoms with a coordination number of 9 at low-index planes [11]. In contrast, O_2 activation barriers are insensitive to Pt atom coordination [13,26]. Thus, the O* removal step, in contrast with the step that forms O* via O_2 dissociation, becomes less facile with decreasing coordination, leading to higher O* coverages at low-coordination sites during CO oxidation catalysis.

The fraction of exposed metal atoms at low-coordination positions (e.g., corners and edges in clusters) increases with decreasing cluster size [27], leading to less reactive O* and more strongly bound adsorbed species on small clusters [13,28]. Thus, large clusters should exhibit a smaller η value via a preferential increase in O* removal rates (step 5, Scheme 1). The measured ratio of exchange rates with CO–$^{18}O_2$–$^{16}O_2$ and $^{18}O_2$–$^{16}O_2$ reactants (η) was indeed smaller on large clusters (η = 0.2, 0.5% wt. Pt/SiO_2, 25 nm clusters; 0.8 kPa CO; 0.7 kPa O_2, 773 K) than on smaller clusters (η = 0.3, 3.3 nm clusters), as expected from the greater abundance of terrace sites on larger clusters (0.64 fraction of terrace sites for 3.3 nm clusters vs. 0.97 for 25 nm clusters, assuming a cuboctahedral geometry [27]).

$^{18}O_2$–$^{16}O_2$ isotopic exchange data on Pt clusters of different size (3.3 and 25 nm clusters) with and without CO co-reactants lead us to conclude that low-coordination Pt atoms, located at corner and edge regions of metal clusters, become decorated with O* species that react with CO* much more slowly than more weakly bound O* at low-index planes. Such a proposal is consistent also with the expected effects of O* and CO* binding strength on the relevant rate and equilibrium constants for elementary steps and with the effects of cluster size on the reversibility of O_2 dissociation steps during CO oxidation catalysis. In the next section, we show how these decoration effects lead to the observed effects of Pt cluster size on CO oxidation turnover rates without concomitant changes

in the CO* binding properties of the surface regions actually involved in catalytic turnovers.

3.6. Cluster size effects on turnover rates and on the rate and equilibrium constants for the relevant elementary steps

The decoration of low-coordinated Pt atoms by strongly-bound and less reactive O* species toward CO oxidation, inferred from the rate and equilibrium constants for elementary steps that mediate CO oxidation catalysis, would obscure any intrinsic effects of surface structure and cluster size on surface reactivity, because low-index surfaces would contribute more to the observed CO_2 products than low-coordination Pt atoms. The effects of Pt dispersion on measured $K_{O_2}k_{Of}$ and K_{CO} values are shown in Fig. 9a and b, respectively, for a series of Pt catalysts with 1.8–25 nm mean cluster diameter (0.2–0.5% wt, Pt/SiO_2; 773 K). Rate and equilibrium constants were determined by regressing the rate data to the functional form of Eq. (12). Since rates are normalized by the total number of exposed Pt atoms (determined by strongly chemisorbed hydrogen uptakes; Section 2.1) O_2 activation rate constant ($K_{O_2}k_{Of}$) but not equilibrium constant for CO adsorption (K_{CO}) is normalized by exposed metal atoms in Eq. (12). The equilibrium constant for CO adsorption (K_{CO}) was essentially independent of Pt cluster size (Fig. 9a); these constant values seem inconsistent at first glance with the expected stronger binding of CO* on small clusters, which expose atoms of lower coordination [27]. CO adsorption constants (K_{CO}) that do not depend on cluster size are, however, consistent with the decoration of surface patches near edges and corners, even though small clusters expose atoms with lower average coordination and stronger bonds with chemisorbed CO [27]. CO desorbs at higher temperatures from small than large clusters [29], a trend consistent with DFT-derived CO adsorption enthalpies on Pt atoms with different coordination (-171 kJ mol^{-1} on corner sites; -162 kJ mol^{-1} on an edge site; -120 kJ mol^{-1} on a (1 1 1) terrace [3] in 201 atom cuboctahedral Pt clusters). Decoration by strongly-bound species during CO oxidation catalysis prevents such sites from contributing to measured rates and therefore to the kinetic or thermodynamic parameters that appear in the rate equation. Measured K_{CO} values reflect those of Pt atoms at low-index terraces where turnovers principally occur and whose fractional abundance but not binding properties depend on Pt cluster size.

In contrast, effective O_2 activation constants ($K_{O_2}k_{Of}$) increased markedly with increasing cluster size for sizes between 1.8 and 8.5 nm and then remained nearly constant on larger Pt clusters (>8.5 nm; Fig. 9b). These O_2 activation rate constants reflect the energy of very early transition states (ubiquitous in exothermic adsorption steps), which are insensitive to surface coordination, because these states cannot sense the stability of the O* products ultimately formed. Therefore, it seems surprising, at first glance, that $K_{O_2}k_{Of}$ values increase sharply with increasing Pt cluster size. At higher temperatures (873 K), when Pt clusters remain essentially bare, $K_{O_2}k_{Of}$ values measured during $CO–O_2$ or $CH_4–O_2$ reactions did not depend on Pt cluster size [13]. Decoration of low-coordination sites by strongly-bound O* makes the number of Pt atoms accessible for turnovers to be smaller than the number of exposed metal atoms (used to normalize rates); thus, O_2 activation constants ($K_{O_2}k_{Of}$) increase because the fraction of the exposed metal atoms that remains accessible for turnovers (atoms at low-index planes) increases with increasing cluster size. Fig. 9b shows the expected increase in the fraction of surface atoms at terrace sites with increasing size of cuboctahedral clusters [27] together with measured $K_{O_2}k_{Of}$ values (per exposed Pt atom). $K_{O_2}k_{Of}$ values and the fraction of atoms at low-index planes both increase with cluster size, but turnover rates reach constant values for larger clusters (3 nm) than the fraction of terrace sites (1 nm, Fig. 9b), suggesting that even terrace sites possibly those vicinal to edges and corners are also covered with less reactive O* species. We indeed find that measured O_2 activation constants ($K_{O_2}k_{Of}$; Fig. 9b) parallel the increase in the fraction of terrace sites, when those immediately adjacent to corner and edge sites are excluded from the estimates (Fig. 9b). The decoration of low-coordination sites by C* or CO* could also lead to the observed effects of cluster size on rate and equilibrium constants, but cannot account for oxygen exchange rates much larger than expected from measured χ values (Section 3.5; $\chi = 4.3 \times 10^{-3}$ on 0.5% wt. Pt/SiO_2, 3.3 nm clusters, 773 K, 0.8 kPa CO, 0.7 kPa O_2; $\eta = 0.2$ and 0.3 measured during $CO–{}^{16}O_2–{}^{18}O_2$ on Pt/SiO_2 25 and 3.3 nm clusters, respectively), which must reflect the presence of less reactive but exchangeable O* at low-coordination sites. Strongly-bound O* on low-coordina-

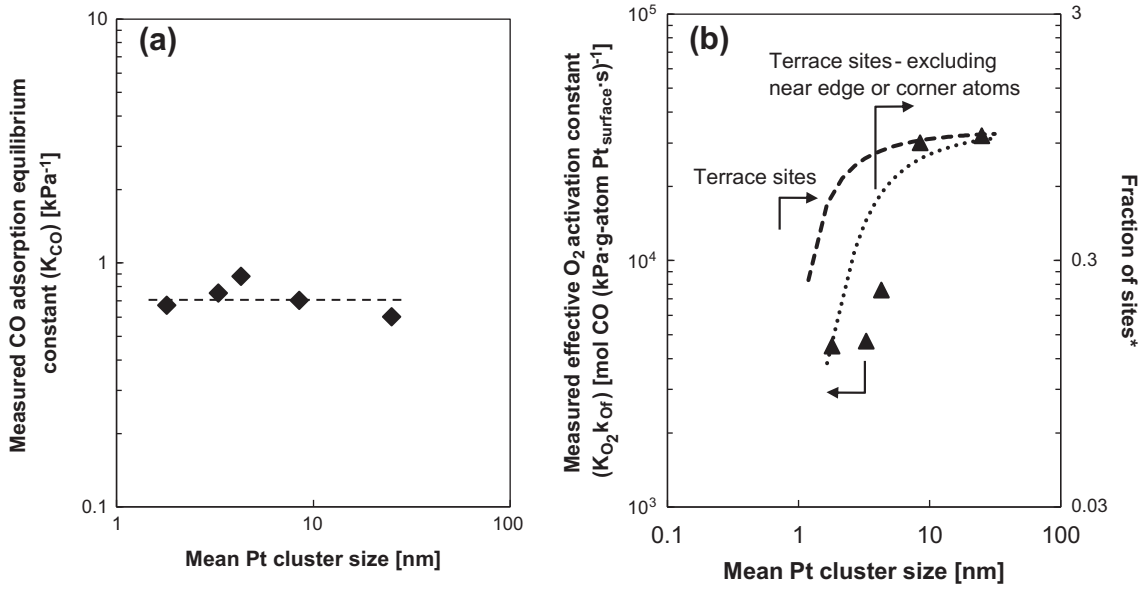

Fig. 9. CO adsorption equilibrium constant ((a); K_{CO}) and effective O_2 activation constant ((b); $K_{O_2}k_{Of}$) on 0.2–0.5% wt. Pt/SiO_2 as a function of mean Pt cluster size diameter (773 K; 300 intraparticle SiO_2/catalyst ratio (λ); 8000 interparticle quartz/catalyst ratio (α); 0.6–0.9 kPa CO; 0.01–0.15 kPa O_2; *fraction of metal atoms at terrace sites (- - -) and at terrace sites excluding atoms close to edge or corner sites (.....); determined from Ref. [27] assuming a cuboctahedral geometry).

Table 3
CO oxidation turnover rates (r_{CO}) on Pt/SiO_2 at low temperature (453 K) before and after CO–O_2 reactions at 773 K.

Temperature (K)	CO oxidation turnover rate [mol CO (g-atom $Pt_{surface}$ − s)$^{-1}$]	
	Mean Pt cluster size	
	1.8 nm [a]	3.3 nm [b]
453[c]	42	50
773[d]	600	730
453[c]	48	54

[a] 0.2% wt. Pt/SiO_2.
[b] 0.5% wt. Pt/SiO_2.
[c] (0.05 kPa CO; 20 kPa O_2).
[d] (0.95 kPa CO; 0.25 kPa O_2).

tion sites exchanges during CO–$^{16}O_2$–$^{18}O_2$ reactions via concerted $^iO_2^*$ reactions with $^jO^*$ (step 7, Scheme 1; i, j = 18 or 16) and lead to higher than expected $^{16}O_2$–$^{18}O_2$ exchange rates (and associated η values; Section 3.5), while decoration by C* or CO* could not account for the $^{16}O_2$–$^{18}O_2$ exchange rates measured during CO oxidation catalysis.

Sintering or inactive adsorbed species, such as C*, that could mimic kinetic effects of cluster size if they occurred predominantly on small clusters, were ruled out by the similar CO oxidation rates measured at 453 K (20 kPa O_2, 0.05 kPa CO), which do not depend on Pt cluster size [3], before and after CO oxidation catalysis at higher temperatures (0.2–0.5% wt. Pt/SiO_2; 0.25 kPa O_2, 0.95 kPa CO) (Table 3). The less exothermic nature of CO adsorption (ΔH_{CO} = −171 kJ mol^{-1}; DFT calculations on bare 201 atom cuboctahedral Pt cluster, 1.8 nm cluster diameter [3]) with respect to oxygen dissociative adsorption (ΔH_O = −426 kJ mol^{-1}; DFT calculations on bare 201 atom cuboctahedral Pt cluster, 1.8 nm cluster diameter [3]), causes CO* coverages to be favored over O* coverages at low temperatures. Strongly-bound O* is not expected to decorate sites at low temperature, since the concomitant increase in CO* coverage with decreasing temperature causes the binding strength of the remaining O* to decrease considerably (change in binding energy for O* on Pt of 113 kJ mol^{-1} from zero CO* coverage to 0.44; DFT calculations for O_2 dissociation on Pt(1 1 1) surfaces at different CO* coverages [22]), and therefore, the strongly-bound oxygen becomes more reactive and is replaced by CO*.

The decoration of low-coordination Pt sites with less reactive O* species during CO oxidation at 723–793 K confers structure sensitivity, by the definition of Boudart [30], to one of the prototypical structure-insensitive reactions. In doing so, these decoration effects preserve a smaller number of exposed atoms in the manifold of reactive sites as the size of Pt clusters decreases. The observed effects of size on rate and thermodynamic constants indicate that CO turnover rates increase with increasing cluster size because low-index planes, with binding properties independent of cluster size, form the majority of the observed CO_2 products. The effects of cluster size on rate and equilibrium constants are consistent with isotopic data (Section 3.5) and with mechanistic interpretations of turnover rates taking place on Pt atoms at low-index planes. The set of elementary steps proposed for CO–O_2 reactions at moderate temperatures (723–793 K) on Pt surfaces partially covered by CO* is also consistent with the transition between the two asymptotic kinetic regimes, in which surfaces are either saturated with CO* (low temperatures: 360–473 K) or bare (high temperatures; >873 K), but where CO oxidation rates are actually independent of Pt cluster size, as we discuss next.

3.7. CO oxidation catalysts throughout its practical temperature range and kinetic consequences of changes in CO* coverages

The effects of CO and O_2 concentration on turnover rates vary throughout the temperature range of interest in CO oxidation catalysis (350–900 K) and specifically as CO* species evolve from saturation coverages to minority species with increasing temperature. Fig. 10 shows concomitant effects of Pt cluster sizes on CO oxidation turnover rates (1.8–25 nm; 2 kPa CO, 1 kPa O_2) at three temperatures (423, 773, and 873 K) where the respective kinetic responses differ.

At low temperatures (360–473 K), CO*-saturated surfaces lead to turnover rates proportional to O_2 pressure and inhibited by CO and to rates limited by O_2^* dissociation assisted by CO* (step 2′, Scheme 1) [3]. Lumped rate and equilibrium constants do not depend on cluster size (Fig. 10), apparently because saturated CO* surfaces dampen the intrinsic non-uniformity of cluster surfaces and its consequences for reactivity [3]. Intermediate temperatures lead to partially covered surfaces and to rates proportional to O_2 pressure and inversely dependent on CO pressure; these kinetic effects reflect kinetically-relevant O_2 dissociation on cluster surfaces partially covered with CO*, as we have shown in the present study. The appearance of vacancy sites at these conditions removes the requirement for assistance by CO* (360–473 K; step 2′, Scheme 1) and allows O_2 dissociation on vacant site pairs (>723 K; step 2, Scheme 1). O* coverages are set by the kinetic coupling between O_2^* dissociation and O* reactions with CO*, in processes that deposit less reactive O* at low-coordination sites and lead to apparent effects of cluster size on turnover rates. Higher temperatures (>873 K) lead to rates proportional to O_2 and unaffected by CO, because O_2 dissociation occurs on vacant sites without detectable competitive adsorption by CO [11]. Turnover rates again become independent of cluster size because O_2 activation proceeds via early transition states characteristic of highly exothermic reactions, which do not sense the binding energy of O-atoms formed as products in O_2 dissociation steps. In traversing such a wide temperature range (350–900 K), we find that the effects of cluster size on CO oxidation turnovers are very weak at high and low temperatures but become quite strong and are much higher on larger clusters at intermediate temperatures. Such diversity in structure sensitivity can be rigorously interpreted in terms of a mechanism that includes a O_2 dissociation as a common rate-limiting step, but on surfaces that become increasingly bare with increasing temperature. These trends show how sensitivity to structure is not a unique property of a named catalytic reaction, but depends, instead, on the nature and kinetic relevance of the elementary steps that mediate such reactions, the nature of which becomes essential in any attempts to interpret or predict the catalytic consequences of cluster size and surface coordination.

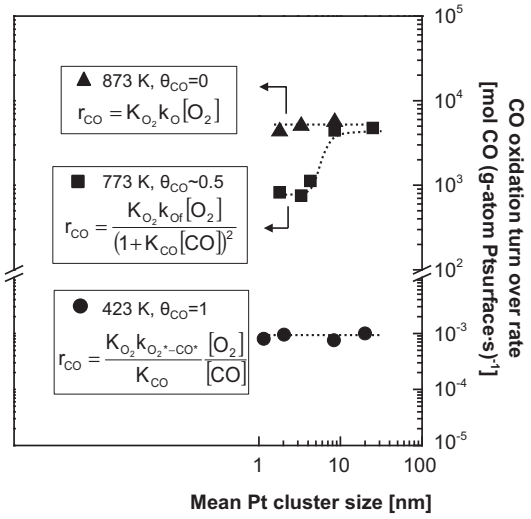

Fig. 10. CO oxidation turnover rates as a function of mean Pt cluster size at 423 K (from Ref. [3]), 773 K, and 873 K (from Ref. [13]) (1 kPa O_2, 2 kPa CO).

4. Conclusions

Kinetic and isotopic assessments of CO–O_2 reactions on Pt (0.2–0.5% wt. Pt/Al_2O_3, 1.8–25 nm) at moderate temperatures (723–793 K) indicate a set of elementary steps in which the kinetically-relevant step is the O_2 dissociation assisted by a vacancy (∗) on a Pt surface partially covered by CO*; consistent with CO oxidation turnover rates that are proportional to O_2 pressures and inhibited by CO pressures. CO oxidation on Pt clusters at intermediate temperatures takes place preferentially on Pt atoms at low-index planes, prevalent on large clusters, since the kinetic coupling between O_2 activation and its reactions with CO* leads to decoration of low-coordinated Pt atoms by strongly-bound and less reactive chemisorbed oxygen atoms. Decoration of low-coordinated Pt atoms by strongly-bound O* lead to surface structure sensitivity and cluster size effects on surface reactivity to CO oxidation reactions, since only a fraction of the exposed atoms (highly coordinated Pt atoms) contributes to the measured CO oxidation turnover rates. These effects account for effective O_2 dissociation rate constants that increase with cluster size as the fraction of Pt atoms at low-index planes concurrently increases, regardless of the lack in structure sensitivity of the highly exothermic O_2 activation steps, which are mediated by very early transition states and do not sense the change in binding strength of the product formed. O* decoration of low-coordination Pt sites also accounts for CO adsorption enthalpies that resemble those of low coordinated sites and are essentially independent of cluster size, in spite of the stronger CO* binding in smaller clusters, since the Pt atoms at which CO oxidation takes place are equivalent. CO oxidation turnover rates that change with cluster size at intermediate temperatures are in sharp contrast with the lack of structure sensitivity for CO oxidation reactions at lower temperatures (360–445 K), for which CO* saturation coverages dampen the intrinsic non-uniformity of cluster surfaces, or at higher temperatures (>873 K), for which non-activated O_2 dissociation steps occur via early transition states that do not sense the ultimate binding strength of the chemisorbed O* products of O_2 dissociation. Hence, these findings show that detailed kinetic data and their mechanistic interpretation at relevant conditions are required for classifying a reaction as sensitive or insensitive to structure.

Acknowledgments

This study has been funded by BP as part of the Methane Conversion Cooperative Research Program at the University of California at Berkeley. M. García-Diéguez acknowledges a postdoctoral fellowship from the Spanish Ministry of Science and Innovation (Mobility Grants for Postdoctoral Research). We also thank Professor David W. Flaherty for helpful technical discussions.

Appendix A. Supplementary material

Supplementary data associated with this article can be found, in the online version, at http://dx.doi.org/10.1016/j.jcat.2013.02.014.

References

[1] M. Rinnemo, D. Kulginov, S. Johansson, K.L. Wong, V.P. Wong, V.P. Zhdanov, B. Kasemo, Surf. Sci. 376 (1997) 297.
[2] F. Joensen, J.R. Rostrup-Nielsen, J. Power Sources 105 (2002) 195.
[3] A.D. Allian, K. Takanabe, K.L. Fujdala, X. Hao, T.J. Truex, J. Cai, C. Buda, M. Neurock, E. Iglesia, J. Am. Chem. Soc. 133 (2011) 4498.
[4] Y.J. Mergler, A. van Aalst, J. van Delft, B.E. Nieuwenhuys, Appl. Catal. B 10 (1996) 245.
[5] B.I. Whittington 1, C.J. Jiang, D.L. Trimm, Catal. Today 26 (1995) 41.
[6] T.V. Choudhary, S. Banerjee, V.R. Choudhary, Appl. Catal. A 234 (2002) 1.
[7] E. Ranzi, A. Frassoldati, S. Granata, T. Faravelli, Ind. Eng. Chem. Res. 44 (2005) 5170.
[8] P.J. Berlowitz, C.H.F. Peden, D.W. Goodman, J. Phys. Chem. 92 (1998) 5213.
[9] S. Ladas, H. Poppa, M. Boudart, Surf. Sci. 102 (1981) 151.
[10] S. Kunz, E. Iglesia, unpublished results.
[11] Y.H. Chin, C. Buda, M. Neurock, E. Iglesia, J. Catal. 283 (2011) 10.
[12] I. Langmuir, Trans. Faraday Soc. 17 (1922) 621.
[13] Y.-H. Chin, C. Buda, M. Neurock, E. Iglesia, J. Am. Chem. Soc. 133 (2011) 15958.
[14] D.M. Nicholas, Y.T. Shah, Ind. Eng. Chem. Prod. Res. Dev. 15 (1976) 35.
[15] R.C. Shishu, L.S. Kowalczyk, Platinum Met. Rev. 18 (1974) 58.
[16] H. Wang, E. Iglesia, ChemCatChem 3 (2011) 1166.
[17] W.M. Haynes, Physical constants of inorganic compounds, in: CRC Handbook of Chemistry and Physics, 91st ed. (Internet Version 2011), CRC Press/Taylor and Francis, Boca Raton, FL, 1991.
[18] R.M. Koros, E.J. Nowak, Chem. Eng. Sci. 22 (1967) 470.
[19] R. Madon, M. Boudart, Ind. Eng. Chem. Fundam. 21 (1982) 438.
[20] W.M. Haynes, Thermodynamic properties as a function of temperature, in: CRC Handbook of Chemistry and Physics, 91st ed. (Internet Version 2011), CRC Press/Taylor and Francis, Boca Raton, FL, 1991.
[21] Ž. Šljivančanin, B. Hammer, Surf. Sci. 515 (2002) 235.
[22] B. Shan, N. Kapur, J. Hyun, L. Wang, J. B Nicholas, K. Cho, J. Phys. Chem. C 113 (2009) 710.
[23] C.E. Wartnaby, A. Stuck, Y.Y. Yeo, D.A. King, J. Phys. Chem. 100 (1996) 12483.
[24] Y.Y. Yeo, L. Vattuone, D.A. King, J. Chem. Phys. 106 (1997) 392.
[25] S.G. Podkolzin, J. Shen, J.J. de Pablo, J.A. Dumesic, J. Phys. Chem. B 104 (2000) 4169.
[26] M. Garcia-Dieguez, Y.H. Chin, E. Iglesia, J. Catal. 285 (2012) 260.
[27] R. Van Hardeveld, F. Hartog, Surf. Sci. 15 (1969) 189.
[28] A. Winkler, X. Guo, H.R. Siddiqui, P.L. Hagans, J.T. Yates Jr., Surf. Sci. 201 (1988) 419.
[29] S. Gan, Y. Liang, D.R. Baer, M.R. Sievers, G.S. Herman, C.H.F. Peden, J. Phys. Chem. B 105 (2001) 2412.
[30] M. Boudart, Chem. Rev. 95 (1995) 661.